INTERNATIONAL JOURNAL OF AUTOMOTIVE AND MECHANICAL ENGINEERING
ISSN: 2229-8649 e-ISSN: 2180-1606
VOL. 20, ISSUE 2, 2023, 10386 – 10397
DOI: https://doi.org/10.15282/ijame.20.2.2023.05.0803

RESEARCH ARTICLE

Taguchi Optimization of Geometrical Factors of a Polymer Composite Patch in Crack Repair

Amol R. Rasane[1,*], Prashant Kumar[2], and Mohan P. Khond[2]

[1]Faculty of Mechanical Engineering, PVG's College of Engineering & SSDIOM, Dindori road, Nashik 422004 (Maharashtra), India
[2]Faculty of Mechanical Engineering, COEP Technological University, Pune 411005 (Maharashtra), India

ABSTRACT - For the repair of a crack in thin aluminium sheets, polymer composite patching is one of the better repair techniques. During service, when the load acts, the patch separates from the substrate due to the stresses developed at the interface. This separation of the patch from the substrate largely depends on the geometrical factors of the patch, i.e. length, width and thickness. The optimum geometrical factors need to be incorporated for the effective and economical repair of the cracks. In this work, the optimum combination of the geometrical factors, i.e. length, width and thickness of the polymer composite patch, is obtained using the Taguchi technique with the help of the results generated in the numerical analyses.

ARTICLE HISTORY
Received : 27th Dec 2022
Revised : 10th May 2023
Accepted : 31st May 2023
Published : 30th June 2023

KEYWORDS
Optimisation
Polymer composite patch
Taguchi technique
Crack repair
Patch separation

1.0 INTRODUCTION

Thin aluminium alloy sheets may have a through-the-thickness crack which grows in the stressed regions under the application of an external load. These cracks propagate with the increase in the applied load, eventually leading to catastrophic failure of the component. The cracks are repaired by bonding a patch made of polymer composites on the cracked region. The bonded patch shares the applied load and prevents crack propagation in the aluminium sheet. But as the applied load increases, the bonded patch starts separating from the aluminium skin due to the interfacial peel and shear stresses. The patch separation is largely influenced by geometrical factors such as patch length, patch width and the number of plies. An optimum combination of these geometrical factors can be obtained by simulating the patch separation process using the finite element method and then analysing the results with a suitable technique such as the Taguchi method.

The repair of metallic structures with composite materials has been investigated by several researchers and was first introduced in Australia in the early 1970s and later in the USA in the early 1980s for the repair of military and civil aircraft [1]. Ratwani [2] studied the structural life enhancement options for airframe structures with a focus on composite patch repair. Okafor et al. [3] performed the stress analysis of a single-sided multi-plies boron/epoxy octagonal composite patch. They observed that the maximum stress in the parent material decreased significantly after the application of the patch. Barroso et al. [4] performed the experiments and analysed the failure of adhesively bonded lap joints between aluminium plates and CFRP laminates by using the local stress state model and studied the influence of plate thickness, CFRP thickness, stacking sequence and overlap length on the failure of the joint. The prediction by local stress state model was compared with that by the numerical method and was found to be satisfactory.

Alfano et al. [5] employed the cohesive zone model to study the Mode-I fracture in a precracked bonded double cantilever beam specimen with the finite element code ABAQUS and examined the sensitivity of cohesive zone parameters in predicting the overall mechanical response. Papathanassiou et al. [6] presented a model for the prediction and optimisation of the composite patch repair applied for the restoration of damaged structures and optimised the bonding process in terms of total procedure duration and energy density consumption by using the genetic algorithm technique. Grabovac and Whittaker [7] applied CFRP patches to the structures used in the ship deck and studied the effectiveness of the bonded repair for a service life of 15 years. Pandey and Kumar [8] observed that the failure criteria selected for predicting the position of the failure in the adhesive for the bonded repair as well as the patch geometry were the important parameters. Ricci et al. [9] performed finite element analysis of the bonded patch repair in case of the fatigue loading and observed that the fatigue life of the metallic plate increases due to the bonding of the patch. M. Ramji et al. [10] concluded that the octagonal patch exhibits better performance in reducing the stress intensity factor among the patches with circular, rectangular, square, elliptical and octagonal shapes. Katnam et al. [11] performed a review on the bonded repair of aircraft structures and identified several scientific challenges and opportunities such as advanced nondestructive testing for damage assessment, advanced surface treatments for interface bonding, controlled cure conditions for patch fabrication, accurate analysis and design for optimised repairs and automation for reliable repairs.

Toudeshky et al. [12] analysed the composite repair of precracked aluminium panels by using cohesive elements and concluded that the separation propagation could be decreased by appropriate dimensional and material properties of the composite patch. Gift et al. [13] studied the role of cohesive zone model in analysing crack propagation in different

*CORRESPONDING AUTHOR | Amol R. Rasane | ramolr2003@yahoo.co.in

materials. Wang et al. [14] carried out one cycle accelerated ageing test on the aluminium structure bonded with composite patch and found that there was no failure in the composite patch as well as the interface between the structure and the patch. Rao et al. [15] presented a detailed overview of the Taguchi method in terms of its evolution, concept, steps involved and its interdisciplinary applications and stated the effectiveness of this method in optimising the products and processes. Sheikh [16] studied the effect of variation of the patch width by performing experiments on a cracked aluminium specimen bonded with a patch made of thin unidirectional GFRP and CFRP plies. Aradhi [17] investigated the patch separation process by using cohesive zone model in the finite element code ANSYS for different lengths of the patch made of unidirectional GFRP and CFRP plies bonded to the cracked aluminium specimen. Shinde et al. [18] concluded from the experiments that until the patch remained bonded to the specimen, the J-integral at the crack tip was small. The separation of the patch was initiated at the crack edge, followed by slow crack growth with the increase in the applied load. The patch failed suddenly after the applied stress exceeded the yield stress of the specimen [19]. Rasane et al. [20] arrived at an optimum combination of patch length and width by generating a response surface from the failure stresses obtained in the numerical analyses performed by using ANSYS 15.0. The current study presents the evaluation of the interface separation between a thin pre-cracked aluminium alloy sheet and a bonded patch made of unidirectional GFRP and CFRP plies. The cohesive zone model was employed in the finite element evaluation and the Taguchi technique was used for optimising the geometrical parameters. An optimum combination of the patch length, patch width and patch thickness were obtained.

2.0 METHODOLOGY

A thin plate of aluminium alloy 6061-T6 with a through-the-thickness centre crack was repaired with a single-sided FRP patch consisting of a thin unidirectional GFRP ply and multiple CFRP plies. Unidirectional tension tests were carried out on a universal testing machine, and the failure loads obtained were compared with the numerical results obtained through finite element analyses. The commercial finite element code ANSYS 15.0 was used for the numerical simulation of the patched specimen, and only a quarter model was analysed due to the symmetric nature of the patched specimen, as shown in Figure 1.

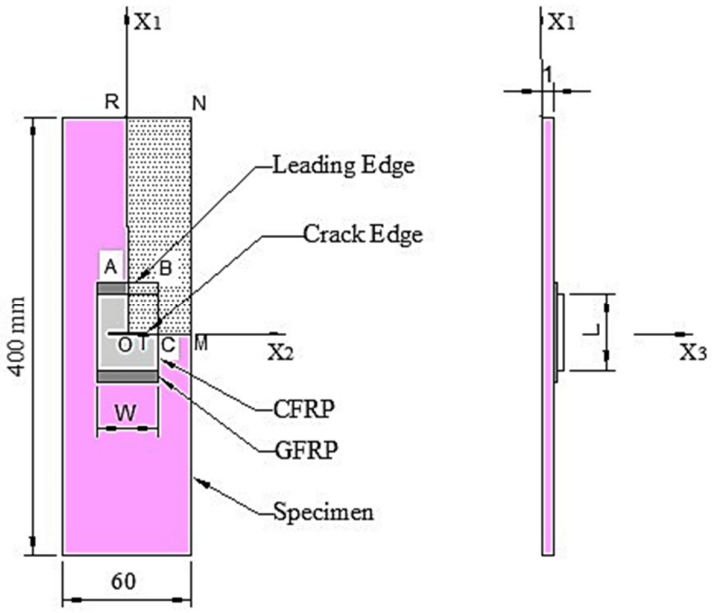

Figure 1. Quarter model of patched specimen

The fracture analysis of the bonded interface between the cracked sheet and composite patch was studied using the cohesive zone material (CZM) model. The CZM model directly introduces fracture mechanism at the interface by adopting softening relationships between tractions and the separations. The interface surfaces of the bonded materials were represented by a special set of interface elements and thus, the CZM model was used to characterise the constitutive behavior of the interface. The cohesive material law with bilinear nature was used to simulate the interface separation process. A mixed mode failure criterion in terms of the normal and tangential separation was specified to describe the failure of the interface. Rasane et al. [20] have shown that the difference between the experimentally and numerically obtained failure stresses was less than 3% confirming the credibility of the numerical method and the cohesive zone model for the analysis of the patch separation process. Sheikh [16] and Shinde [18, 19] have shown through experiments that the patch separation occurred at the interface of the skin and the GFRP ply. Normal and shear stresses, developed at the interface between the aluminium skin surface and the GFRP ply of the patch, initiate the separation of the patch. The separation area increased gradually with the increase in the applied load. This growth was slow and contained until the

applied stress reached the yield stress of the aluminium skin. Once the yield stress of the skin was exceeded, there was rapid growth of the separation area, as shown in Figure 2.

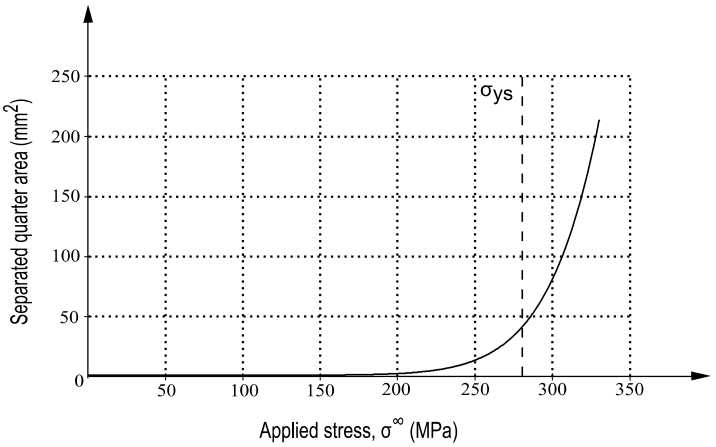

Figure 2. Separation area vs applied stress

A number of numerical simulations were performed for various combinations of the geometrical factors. The width of the patch was varied as 30 mm, 36 mm, 42 mm and 48 mm, while the length of the CFRP ply was varied as 30 mm, 40 mm, 50 mm and 60 mm. The length of the GFRP ply was kept 20 mm longer than that of the longest CFRP ply for all cases. The thickness of the ply varied from one to three CFRP plies. A total of 48 numerical experiments were performed. Thus, there are three parameters for optimisation; length, width & thickness of the patch. The increase in length, width and thickness of the patch resulted in an increase in strength of the patch. But increasing the parameters beyond a certain value may not be possible due to practical constraints, e.g. if enough space is not available for increasing the patch length in the practical application, then it is convenient to increase the thickness so as to obtain a similar strength. Thus, it is appropriate to determine the optimum combination of the dimensional parameters.

3.0 TAGUCHI ANALYSIS

Taguchi method with orthogonal arrays was used for the optimisation of the geometrical factors in the patch separation process. Taguchi method is used in industries for the robust design of products and processes wherein the product/process designed works well under various operating conditions. The robust design is based on three functions, i.e. orthogonal array, S/N ratio and loss function. The Taguchi method involves performing matrix experiments using special matrices called orthogonal arrays to determine the effects of several parameters efficiently. Depending on the number of factors and the factor levels, a suitable orthogonal array is selected. The signal-to-noise ratio of the output responses for all the experiments is determined, and the S/N ratio is maximised to obtain the optimum condition [21, 22, 23]. L48 Taguchi orthogonal array [24] was used in this study with different combinations of the geometrical factors, i.e. patch length, width and thickness, as shown in Table 1. The following parameters were used;

W = width of patch in mm
LGFRP = Length of GFRP ply in mm
LGFRP 1 = length of first CFRP ply in mm
LGFRP 2 = length of second CFRP ply in mm
LGFRP 3 = length of third CFRP ply in mm
n = Number of CFRP plies

The 48 experiments were grouped into 12 sets by combining similar types of experiments together, as shown in Table 2. Factor ‘A’, representing the patch length, was assigned to column 1 of the orthogonal array. Twelve levels were formed for the factor ‘A’ consisting of the patch lengths 30, 40, 50, and 60 mm with single ply; 30, 40, 50, and 60 mm with two plies and 30, 40, 50, and 60 mm with three plies. Thus, there were four levels of single-ply patches, four levels of two plies patches and four levels of three plies patch system. The thickness effect was included in the patch length factor while combining the length groups. The factor ‘B’ representing the patch width was assigned to the second column of the orthogonal array. Four levels of factor ‘B’ were 30, 36, 42 and 48 mm. The other factors C, D, in the orthogonal array were not used in this analysis.

Table 1. L48 orthogonal array [24]

Sr no	1	2	3	4	5	6	7	8	9	10
Expt No	CC1P_1	CC1P_2	CC1P_3	CC1P_4	CC1P_5	CC 1P_6	CC1P_7	CC1P_8	CC1P_9	CC1P_10
W	30	30	30	30	36	36	36	36	42	42
L_{GFRP}	50	60	70	80	50	60	70	80	50	60
L_{CFRP1}	30	40	50	60	30	40	50	60	30	40
L_{CFRP2}	0	0	0	0	0	0	0	0	0	0
L_{CFRP3}	0	0	0	0	0	0	0	0	0	0
n	1	1	1	1	1	1	1	1	1	1
Sr no	11	12	13	14	15	16	17	18	19	20
Expt no	CC1P_11	CC1P_12	CC1P_13	CC1P_14	CC1P_15	CC1P_16	CC2P_1	CC2P_2	CC2P_3	CC2P_4
W	42	42	48	48	48	48	30	30	30	30
L_{GFRP}	70	80	50	60	70	80	50	60	70	80
L_{CFRP1}	50	60	30	40	50	60	30	40	50	60
L_{CFRP2}	0	0	0	0	0	0	20	30	40	50
L_{CFRP3}	0	0	0	0	0	0	0	0	0	0
n	1	1	1	1	1	1	2	2	2	2
Sr no	21	22	23	24	25	26	27	28	29	30
Expt no	CC2P_5	CC2P_6	CC2P_7	CC2P_8	CC2P_9	CC2P_10	CC2P_11	CC2P_12	CC2P_13	CC2P_14
W	36	36	36	36	42	42	42	42	48	48
L_{GFRP}	50	60	70	80	50	60	70	80	50	60
L_{CFRP1}	30	40	50	60	30	40	50	60	30	40
L_{CFRP2}	20	30	40	50	20	30	40	50	20	30
L_{CFRP3}	0	0	0	0	0	0	0	0	0	0
n	2	2	2	2	2	2	2	2	2	2
Sr no	31	32	33	34	35	36	37	38	39	40
Expt no	CC2P_15	CC2P_16	CC3P_1	CC3P_2	CC3P_3	CC3P_4	CC3P_5	CC3P_6	CC3P_7	CC3P_8
W	48	48	30	30	30	30	36	36	36	36
L_{GFRP}	70	80	50	60	70	80	50	60	70	80
L_{CFRP1}	50	60	30	40	50	60	30	40	50	60
L_{CFRP2}	40	50	20	30	40	50	20	30	40	50
L_{CFRP3}	0	0	10	20	30	40	10	20	30	40
n	2	2	3	3	3	3	3	3	3	3
Sr no	41	42	43	44	45	46	47	48		
Expt no	CC3P_9	CC3P_10	CC3P_11	CC3P_12	CC3P_13	CC3P_14	CC3P_15	CC3P_16		
W	42	42	42	42	48	48	48	48		
L_{GFRP}	50	60	70	80	50	60	70	80		
L_{CFRP1}	30	40	50	60	30	40	50	60		
L_{CFRP2}	20	30	40	50	20	30	40	50		
L_{CFRP3}	10	20	30	40	10	20	30	40		
n	3	3	3	3	3	3	3	3		

Table 2. Modified L48 orthogonal array

Level	1	1	1	1	2	2	2	2
Expt no	CC1P_1	CC1P_5	CC1P_9	CC1P_13	CC1P_2	CC1P_6	CC1P_10	CC1P_14
Level	3	3	3	3	4	4	4	4
Expt no	CC1P_3	CC1P_7	CC1P_11	CC1P_15	CC1P_4	CC1P_8	CC1P_12	CC1P_16
Level	5	5	5	5	6	6	6	6
Expt no	CC2P_1	CC2P_5	CC2P_9	CC2P_13	CC2P_2	CC2P_6	CC2P_10	CC2P_14
Level	7	7	7	7	8	8	8	8
Expt no	CC2P_3	CC2P_7	CC2P_11	CC2P_15	CC2P_4	CC2P_8	CC2P_12	CC2P_16
Level	9	9	9	9	10	10	10	10
Expt no	CC3P_1	CC3P_5	CC3P_9	CC3P_13	CC3P_2	CC3P_6	CC3P_10	CC3P_14
Level	11	11	11	11	12	12	12	12
Expt no	CC3P_3	CC3P_7	CC3P_11	CC3P_15	CC3P_4	CC3P_8	CC3P_12	CC3P_16

The standard L48 Taguchi orthogonal array was used, as shown in the Table T1 of Appendix. From the results of the numerical analysis, the output response was obtained as the normal stresses (Y) in the skin at the origin and at the point where the inner ply was touching the skin. The normal stress (Y) is shown in Table T2 of Appendix. The interfacial normal and shear stresses (σin and σis) as well as the separation distance, were also obtained. The next step in the Taguchi method is to determine the signal-to-noise ratio known as the S/N ratio. The S/N ratio is a measurement scale that represents the ratio of sensitivity to variability. There are two types of the S/N ratio: static and dynamic. The patch separation process was analysed by using static as well as dynamic S/N ratios based on three criteria; linearity, critical load and the volume of the patch. The static S/N ratio was used for the critical load and the volume of the patch while the dynamic S/N ratio was used for the linearity check. The P diagram for the dynamic case is shown in Figure 3 [22].

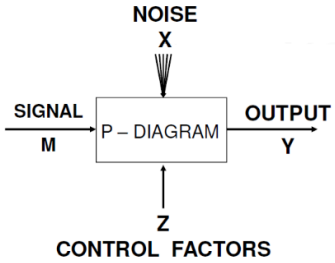

Figure 3. P-diagram for dynamic problems [22]

The signal factors (M) are the parameters set by the user of the process to express the intended value for the output/response (Y) of the product. The noise factors (X) are the factors that are difficult to control in the field, and they cause the output (Y) to deviate from the target specified by the signal factor. The control factors (Z) are the parameters that can be specified freely by the designer. In a measurement system, the input-to-output relationship is studied. In a good measuring system, the response of measurement must be proportional to the true value. In a dynamic system, there is always a need to adjust the output to the target by varying a certain input signal. In such a case, adjustability becomes critical for the design. Here it is important that the input/output relationship be proportional or linear. In other words, linearity becomes critical for adjusting systems. The better the linearity and the steeper the input/output relationship, the better the adjustability. A good measurement system must be sensitive to different inputs; thus, the slope showing the input/output relationship must be steep. Therefore, the slope is used as being equivalent to sensitivity. The variability also must be small. For the patch separation process, the S/N ratio of the type continuous–continuous, i.e. both the input and the output as continuous variables, was used. When a dynamic S/N ratio is used to evaluate a measuring system, the three elements, sensitivity, slope and variability, are combined into a single index, S/N ratio allowing the user to evaluate and improve the system. The linearity between the signal factor and the output response was verified by using the dynamic S/N ratio in terms of the slope (β) given by [22, 23];

$$\eta = 10 * \log_{10}(\beta^2) \quad (1)$$

To verify the linearity between the input (applied stress, M) and the output (normal stress developed in the patch, Y), the relation of normal stress in the patch against the applied stress in the axial direction was plotted for all 48 cases. The input/output relation for the case of a single patch with a length of 30 mm and width of 30 mm with four distinct points is shown in Figure 4.

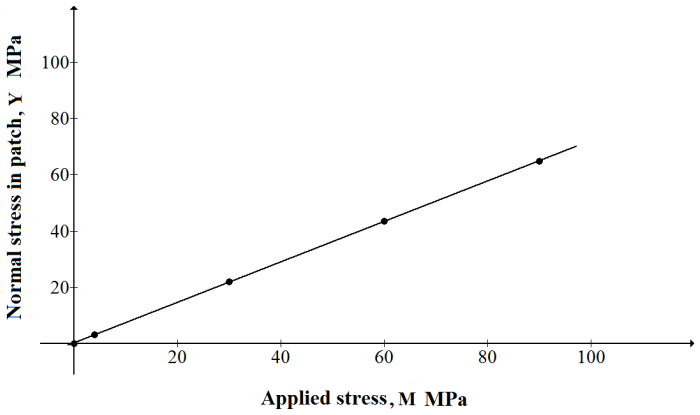

Figure 4. Input-output linear characteristics

From the figure, it was clear that there was a linear relationship between the applied stress and the normal stress in the patch for four distinct points. The same linear relationship was observed for all the remaining cases. This implied that the skin-patch assembly followed a linear relation under the action of applied load similar to a solid material. Thus the patch separation process satisfied the linearity criterion as per the Taguchi technique. It was also observed from the graph that the variability around the linear curve of the input/output was very small for all the cases, satisfying the criterion of the variability of the Taguchi technique.

Though the sensitivity was not important in this case, it was checked. To check the sensitivity between the input and output, the slope of the straight line in the above graph of normal stress against the applied stress was determined, and the S/N ratio for the slope was calculated for all the cases by using Eq. (1) as shown in Table T3 of Appendix. By using the S/N ratios obtained and by performing analysis of variance (ANOVA), the factor effects were calculated for each factor and the factor effect plot for the slope was generated in the MS Excel software, as shown in Figure 5.

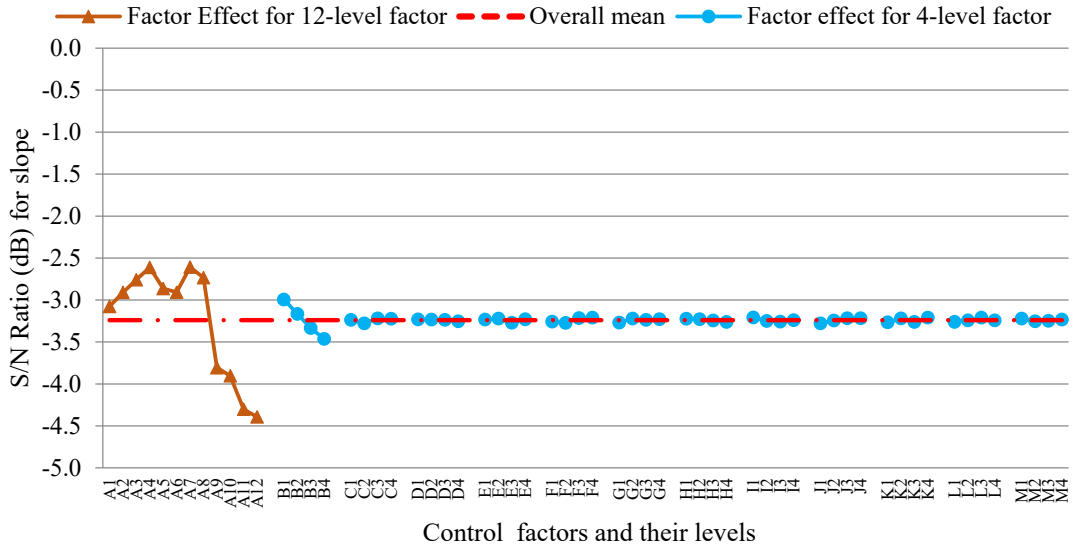

Figure 5. Factor effect plot for slope characteristics

From the factor effect plot of the slope characteristics, it was observed that the two maximum S/N ratio values for the factor 'A' were -2.609 and -2.735, corresponding to the levels A7 and A8 respectively, in the two plies system. The maximum S/N ratio for the factor 'B' was obtained as -2.995, corresponding to level B1. With these maximum S/N ratios, the high sensitivity was verified. The main objective with the slope characteristics was to verify the linearity between applied stress as input and normal stress as output. In four-level factors, the width remains constant, but the length varies for the selected level. Since at the given level the thickness remains constant, there is no variation in the S/N ratio.

The other objective of the optimisation was to minimise the amount of material used in the crack repair, which was expressed in terms of the volume of the patch. For obtaining the minimum volume condition, a static S/N ratio with a smaller the better criterion was used. The P diagram for the static case is shown in Figure 6.

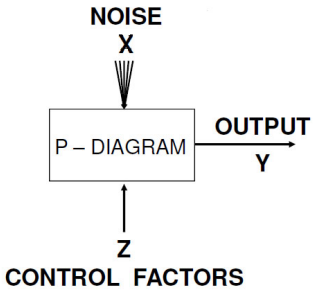

Figure 6. P-diagram for static problems [22]

The static S/N ratios are used to study a single target, and it includes two aspects; sensitivity and variability. In the design of a product for a fixed target, there is no need to adjust the target from time to time, and the mean is considered as being equivalent to sensitivity. The value of the S/N ratio is expressed in terms of a decibel value. To express S/N ratio in decibel form, the logarithm of the mean sum of squares is multiplied by -10; that is:

$$\eta = -10 * \log_{10}(\text{mean of sum of squares}) \quad (2)$$

The S/N ratio for volume was calculated by using Eq. (2) as shown in Table T4 of Appendix. By using the S/N ratios obtained and by performing the analysis of variance (ANOVA), the factor effects were calculated for each factor and the factor effect plot for volume was generated in the MS Excel software as shown in Figure 7.

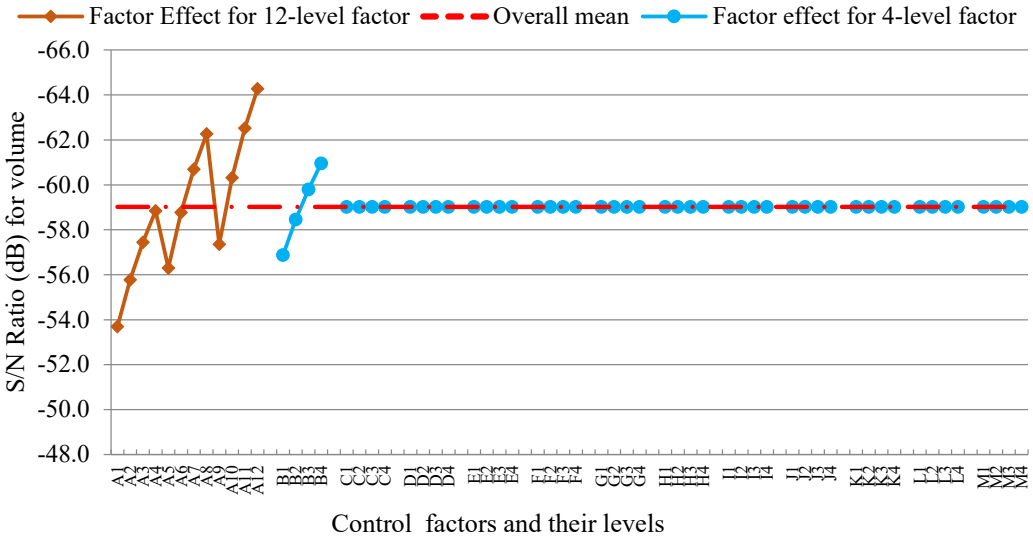

Figure 7. Factor effect plot for volume

For volume characteristics, the criterion of smaller the better was applied. From the factor effect plot for volume, it was observed that the S/N ratio was at the maximum at -62.268 for level A8 in the two plies system while it was the maximum at -64.278 for level A12 in the three plies system for the factor 'A'. The S/N ratio was at the maximum at the level 'B4', and it was -60.957 for the factor 'B'. In 4-level factors, the width remains constant, but the length varies for the selected level. Since, at the given level, the thickness remains constant, there is no variation in the S/N ratio.

Then the criterion of the critical load of separation of the patch was applied. Since the critical load associated with the complete failure of the patch needed to be maximised since it delays the failure of the patch, the larger-the-better criterion was used, and the corresponding S/N ratio was obtained. The S/N ratio for the larger-the-better condition is expressed in terms of a decibel value. To express the S/N ratio in decibel form, the logarithm of the mean of the sum of reciprocals squares was multiplied by -10; that is:

$$\eta = -10 * \log_{10} (\text{mean of sum of reciprocals squares}) \quad (3)$$

To maximise the critical load, the S/N ratio values for the critical load (Pc) were determined by using the Eq. (3) and are shown in Table T5 of Appendix. By using the S/N ratio and by performing the analysis of variance (ANOVA), the factor effects were calculated for each factor and the factor effect plot for the critical load was generated in the MS Excel software, as shown in Figure 8.

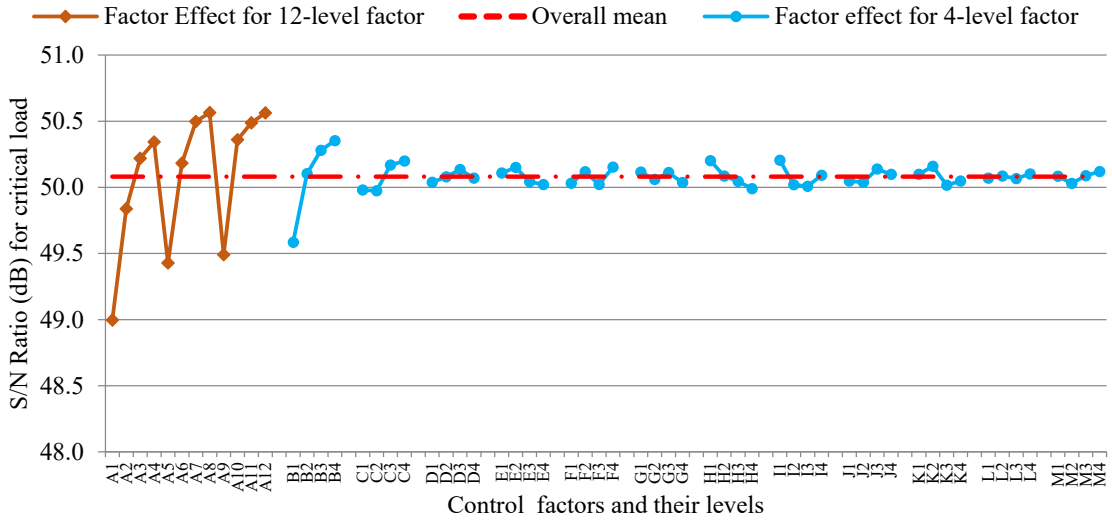

Figure 8. Factor effect plot for the critical load

For the critical load characteristics, the larger the better criterion was used. From the factor effect plot, it was observed that the S/N ratio was at the maximum at level A8 of the two plies system. It was also the maximum at level A12 of the three-plies system. The S/N ratio for A8 and A12 were 50.565 and 50.563, respectively. Even if three CFRP plies are

used for arresting the crack propagation, there is hardly any improvement in the critical loads, i.e. the load at which there is complete failure of the patch. The two plies and the three plies patches have the same strength from the separation point of view, and increasing the number of plies above the two plies system only increases the volume of the patch. For economical repair, the two plies patch proves to have sufficient strength. Thus, with the critical load criterion, the maximum S/N ratio was considered at level A8 of the two plies patch. For factor B, the maximum S/N ratio was at level B4. It was observed to be 50.353.

For optimising the patch geometry, all the above criteria were considered and the optimum conditions were obtained, which can be summarised as follows. As per the slope characteristics criterion, level A8 of the factor 'A' satisfied the condition for the slope characteristics. As per the patch volume criterion, level A8 in two plies system and A12 in three plies system satisfied the volume criteria. Since the two plies condition provided sufficient strength as per the critical load condition, the level A12 of three plies patch was not considered, and it was discarded. As per the critical load criterion, level A8 of the two plies system gave the maximum S/N ratio corresponding to the critical load. Thus, from the above discussion, it was clear that level A8 satisfied all the criteria required for the economical and efficient repair of the crack. So, level A8 was chosen as the optimum level of factor 'A' for the patch separation process. Level A8 had four combinations of the geometrical parameters labelled as CC2P_4, CC2P_8, CC2P_12 and CC2P_16. One level out of these four was to be selected as the optimum level. CC2P_4, CC2P_8, CC2P_12 and CC2P_16 had the S/N ratio of 50.543, 50.565, 50.572 and 50.580, respectively. The failure stress corresponding to the numerical non-convergence in the finite element analysis was nearly the same for these cases, with a negligible difference, as seen from Table T5 of Appendix A. Any combination of these four can be considered as the optimum one with the critical load criterion. The combination CC2P_4 satisfied the slope condition, and it had the minimum patch volume at 1014 mm3. So CC2P_4 was considered as the optimum combination for the patch separation process based on the factor effect of factor 'A'. The patch length corresponding to this level was 60 mm, with two CFRP plies having a patch width of 30 mm.

For the 4-level factor B, level B1 satisfied the requirement of the slope characteristics. As per the volume criterion and the critical load criterion, factor level B4 satisfied the necessary requirements. Since the slope was used only to verify the linearity between the input and the output, the value of the slope did not matter in this case. The other two criteria, the smaller volume and the larger critical load were more important for the patch separation process. So factor level B4 was considered to be the optimum level for factor B based on the volume and the critical load criteria. Factor level B4 had twelve combinations with a patch width of 48 mm contributing to its effect on the patch separation process. The combination CC1P_14 satisfied both the conditions, i.e. maximum critical load at 332.8 MPa and the minimum volume 768 mm^3 among all the combinations of factor B4. The dimensions for this combination were: patch width = 48 mm, patch length = 40 mm and number of plies = 1.

From the analysis of variance (ANOVA) based on the critical load criterion, the contribution of factor A (71%) was greater than the contribution of factor B (25%). So, based on the critical load criterion, the optimum combination was predicted as CC2P_4 with the patch length 60 mm, patch width 30 mm and two numbers of CFRP plies. Based on the volume criterion, the combination CC1P_14 having the minimum volume was considered as the optimum combination with the patch length of 40 mm, patch width of 48 mm and a single CFRP ply. The optimum combination based on both the criterion, i.e. critical load and the volume, was obtained by combining the two experiments, CC2P_4 and CC1P_14. Thus, from the factor effect study of the factors 'A' and 'B', the optimum geometrical factors for the patch separation process were determined, as shown in Table 3. With this optimum combination, the verification experiment was performed, and it was observed that the critical load obtained was 338.05 MPa. The range of the critical load predicted by the analysis of variance was 334.5 MPa to 362.2 MPa. It was clear that the critical load of the verification experiment was in the predicted range, and it was acceptable. The volume of the patch for the optimum combination was 1622.4 mm^3. The input-output relation was observed to be linear.

Table 3. Optimum geometrical factors

Optimum patch length (mm)	Optimum patch width (mm)	Number of plies	Critical load (MPa)	Volume (mm^3)
60 mm	48 mm	2	338.05	1622.4

Thus, the Taguchi technique was successfully applied to optimise the geometrical factors of the patch separation process.

4.0 CONCLUSIONS

This study was carried out to determine the optimum patch size for a through-the-thickness centre crack repaired with a polymer composite patch in a thin aluminium alloy sheet. Numerical analyses were carried out using the cohesive zone model by varying the patch width from 30 mm to 48 mm, patch length from 30 mm to 60 mm and the number of plies from one to three. The variation of the stresses in the patch separation process was obtained. Taguchi analysis was used to plot the factor effect plots. The linearity, sensitivity and variability between the applied stress and the normal stress developed in the patch were checked. The condition for the maximum critical load was ensured and finally, the patch

with the minimum volume was selected as the optimum patch. The optimum geometrical factors were obtained as; patch width of 48 mm, patch length of 60 mm with two plies.

5.0 ACKNOWLEDGEMENT

This study was supported by Structures Panel of Aeronautics Research and Development Board (ARDB), Defense Research and Development Organization (DRDO), New Delhi, India.

6.0 REFERENCES

[1] Duong Cong N. and Wang Chun Hui, *Composite Repair – Theory & Design*, Netherlands: Elsevier, 2007.
[2] M. Ratwani, "Repair options for airframes," Defense Technical Information Center Compilation Part Notice, RTO EN 015, Bulgaria, 2000.
[3] Okafor Chukwujekwu, Singh Navdeep, U.E. Enemuoh, and S.V. Rao, "Design, analysis and performance of adhesively bonded composite patch repair of cracked aluminium aircraft panels," *Composite Structures*, vol. 71, pp. 258 – 270, 2005.
[4] A. Barroso, F. Paris, and V. Mantic, "Failure of adhesively bonded joints: analysis of experimental results by nominal and local approaches," *Projects TRA2005-06764*, Spanish Ministry of Education and Science, 2005.
[5] M. Alfano, F. Furgiuele, A. Leonardi, C. Maletta and G. H. Paulino, "Cohesive zone modeling of mode I fracture in adhesive bonded joints," *Key Engineering Material,* vol. 348-349, pp 13 – 16, 2007.
[6] Th. K. Papathanassiou, S. P. Filopoulos, and G. J. Tsamasphyros, "Optimisation of composite patch repair processes with the use of genetic algorithms," In International Conference on Engineering Optimisation, Brazil, 2008.
[7] I. Grabovac and W. David, "Application of bonded composites in the repair of ship structures – A 15 years' service experience," *Composites Part A,* vol. 40, pp. 1 – 18, 2009.
[8] P.C. Pandey and Kumar S., "Adhesively-bonded patch repair with composites," *Defence Science Journal*, vol. 60-3, pp. 320-329 (2010).
[9] R. Fabrizio, F. Francesco and M. Nicola, "Bonded composite patch repairs on cracked aluminum plates: Theory, modeling and experiments," in *Advances in composite materials – Ecodesign and Analysis*, Brahim Attaf, Ed., Intech Open, 2011, pp. 457-476.
[10] M. Ramji, R. Srilakshmi, and M. BhanuPrakash, "Towards optimisation of patch shape on the performance of bonded composite repair using FEM," *Composites - Part B,* vol. 45, pp. 710 – 720, 2013.
[11] K.B. Katnam, L.F.M. Da Silva, and T.M. Young, "Bonded repair of composite aircraft structures: a review of scientific challenges and opportunities," *Progress in Aerospace Sciences*, vol. 61, pp. 26 – 42, 2013.
[12] H.H. Toudeshky, A. Jasemzadeh, and B. Mohammadi, "Investigation of effective parameters on composite patch debonding under static and cyclic loading using cohesive elements," *Finite Elements in Analysis and Design*, vol. 74, pp. 67 – 75, 2013.
[13] M.D. Mohan Gift, P. Selvakumar, and S. John Alexis, "A review on the cohesive zone models for crack propagation analysis," *Elixir Mechanical Engineering*, vol. 55, pp. 12760 – 12763, 2013.
[14] W. Zun, Z. Yishan, X. Jun and Y. Wei, "Effect of accelerated ageing on the mechanical properties of composite repaired aluminium plates," In International Conference on Quality, Reliability, Risk, Maintenance, and Safety Engineering, pp. 863 – 866, 2013.
[15] S. Rao, P. Saman, A. Kadampatta, and R. Shenoy, "An overview of Taguchi method: evolution, concept interdisciplinary applications," *International Journal of Scientific and Engineering Research*, vol 4, no. 10, pp. 621 – 626, 2013.
[16] S. Syed, "Development of a reusable pin loading fixture to study the effect of patch width bonded on a cracked specimen," M.Tech thesis, Department of Mechanical Engineering, College of Engineering Pune, India, 2015.
[17] A. Sudhindra, "Debond Characterization of a thin cracked plate repaired with an frp patch using the cohesive zone material model," M.Tech (Mechanical Engg) Thesis, College of Engineering Pune, India, 2015.
[18] Shinde P. S, Kumar P, Singh K. K, Tripathi V. K, and Sarkar P. K., "Experimental Study of CFRP patches bonded on a cracked Aluminum alloy panel," *Composite Interfaces*, vol. 22/4, pp. 233-248, 2015.
[19] Shinde P. S, Kumar P, Singh K. K, Tripathi V. K, Aradhi S. and Sarkar P. K., "The role of yield stress on cracked thin panels of aluminium alloys repaired with an FRP patch," *The Journal of Adhesion*, vol.93-5, pp.412-429, 2015.
[20] A.R. Rasane, P. Kumar, and M.P. Khond, "Optimising the size of a CFRP patch to repair a crack in a thin sheet," *The Journal of Adhesion*, vol.93-13, pp.1064-1080, 2016.
[21] J. Ross Philip, "Taguchi techniques for quality engineering," New Delhi: McGraw Hill Education Pvt Ltd, 2014.
[22] S. P. Madhav, "Quality engineering using robust design," India: Pearson Publications Noida (U.P.), 2009.
[23] G. Taguchi, S. Chowdhury, Y. Wu, "Taguchi's quality engineering handbook," Hoboken: John Wiley & Sons, 2005.
[24] P.R. Apte [Online]. Available: www.ee.iitb.ac.in / ~ apte http://support.sas.com/techsup/technote/ts723_Designs.txt [Accessed May 25, 2017].

7.0 APPENDIX

The appendix contains the standard L48 orthogonal array and the output, i.e. stresses obtained from numerical analysis and S/N ratio obtained by using Taguchi technique.

Table T1. Standard L48 Taguchi orthogonal array [24]

A	B	C	D	E	F	G	H	I	J	K	L	M
A1	B1	C1	D1	E1	F1	G1	H1	I1	J1	K1	L1	M1
A1	B2	C2	D2	E2	F2	G2	H2	I2	J2	K2	L2	M2
A1	B3	C3	D3	E3	F3	G3	H3	I3	J3	K3	L3	M3
A1	B4	C4	D4	E4	F4	G4	H4	I4	J4	K4	L4	M4
A2	B1	C1	D1	E3	F3	G3	H4	I4	J4	K2	L2	M2

A2	B2	C2	D2	E4	F4	G4	H3	I3	J3	K1	L1	M1
A2	B3	C3	D3	E1	F1	G1	H2	I2	J2	K4	L4	M4
A2	B4	C4	D4	E2	F2	G2	H1	I1	J1	K3	L3	M3
A3	B1	C1	D1	E4	F4	G4	H2	I2	J2	K3	L3	M3
A3	B2	C2	D2	E3	F3	G3	H1	I1	J1	K4	L4	M4
A3	B3	C3	D3	E2	F2	G2	H4	I4	J4	K1	L1	M1
A3	B4	C4	D4	E1	F1	G1	H3	I3	J3	K2	L2	M2
A4	B1	C2	D4	E1	F3	G2	H2	I3	J4	K4	L3	M1
A4	B2	C1	D3	E2	F4	G1	H1	I4	J3	K3	L4	M2
A4	B3	C4	D2	E3	F1	G4	H4	I1	J2	K2	L1	M3
A4	B4	C3	D1	E4	F2	G3	H3	I2	J1	K1	L2	M4
A5	B1	C2	D4	E2	F1	G3	H3	I4	J2	K1	L4	M3
A5	B2	C1	D3	E1	F2	G4	H4	I3	J1	K2	L3	M4
A5	B3	C4	D2	E4	F3	G1	H1	I2	J4	K3	L2	M1
A5	B4	C3	D1	E3	F4	G2	H2	I1	J3	K4	L1	M2
A6	B1	C2	D4	E3	F2	G1	H4	I2	J3	K3	L1	M4
A6	B2	C1	D3	E4	F1	G2	H3	I1	J4	K4	L2	M3
A6	B3	C4	D2	E1	F4	G3	H2	I4	J1	K1	L3	M2
A6	B4	C3	D1	E2	F3	G4	H1	I3	J2	K2	L4	M1
A7	B1	C3	D2	E1	F2	G4	H1	I4	J3	K4	L2	M3
A7	B2	C4	D1	E2	F1	G3	H2	I3	J4	K3	L1	M4
A7	B3	C1	D4	E3	F4	G2	H3	I2	J1	K2	L4	M1
A7	B4	C2	D3	E4	F3	G1	H4	I1	J2	K1	L3	M2
A8	B1	C3	D2	E2	F4	G1	H3	I1	J4	K2	L3	M4
A8	B2	C4	D1	E1	F3	G2	H4	I2	J3	K1	L4	M3
A8	B3	C1	D4	E4	F2	G3	H1	I3	J2	K4	L1	M2
A8	B4	C2	D3	E3	F1	G4	H2	I4	J1	K3	L2	M1
A9	B1	C3	D2	E4	F1	G2	H4	I3	J1	K3	L4	M2
A9	B2	C4	D1	E3	F2	G1	H3	I4	J2	K4	L3	M1
A9	B3	C1	D4	E2	F3	G4	H2	I1	J3	K1	L2	M4
A9	B4	C2	D3	E1	F4	G3	H1	I2	J4	K2	L1	M3
A10	B1	C4	D3	E2	F3	G4	H3	I2	J1	K4	L1	M2
A10	B2	C3	D4	E1	F4	G3	H4	I1	J2	K3	L2	M1
A10	B3	C2	D1	E4	F1	G2	H1	I4	J3	K2	L3	M4
A10	B4	C1	D2	E3	F2	G1	H2	I3	J4	K1	L4	M3
A11	B1	C4	D3	E3	F4	G2	H1	I3	J2	K1	L2	M4
A11	B2	C3	D4	E4	F3	G1	H2	I4	J1	K2	L1	M3
A11	B3	C2	D1	E1	F2	G4	H3	I1	J4	K3	L4	M2
A11	B4	C1	D2	E2	F1	G3	H4	I2	J3	K4	L3	M1
A12	B1	C4	D3	E4	F2	G3	H2	I1	J3	K2	L4	M1
A12	B2	C3	D4	E3	F1	G4	H1	I2	J4	K1	L3	M2
A12	B3	C2	D1	E2	F4	G1	H4	I3	J1	K4	L2	M3
A12	B4	C1	D2	E1	F3	G2	H3	I4	J2	K3	L1	M4

Table T2. Normal stress in the patch at different applied stresses

Level	Expt no	Normal stress (Y) in patch (MPa) for the specified applied stress (M), MPa											
		0	4	30	60	90	120	150	180	210	240	270	300
1	CC1P_1	0	3.18	21.96	43.46	64.86	89.60	143.62	155.97	163.55	156.33	150.23	----
1	CC1P_5	0	3.15	21.66	42.81	63.83	88.07	143.13	155.93	162.77	153.06	155.30	135.31
1	CC1P_9	0	3.13	21.45	42.34	63.08	86.95	141.16	155.21	163.31	165.49	157.29	130.20
1	CC1P_13	0	3.11	21.29	41.98	62.49	86.08	139.66	154.88	161.25	157.79	157.60	129.20
2	CC1P_2	0	3.27	22.55	44.64	66.61	91.97	146.82	166.39	177.17	169.61	180.16	179.39
2	CC1P_6	0	3.22	22.13	43.74	65.20	89.91	143.79	165.40	173.72	177.78	171.32	168.35
2	CC1P_10	0	3.18	21.82	43.06	64.12	88.34	141.19	162.02	175.65	175.86	170.49	171.38
2	CC1P_14	0	3.16	21.58	42.53	63.27	87.10	139.07	161.01	172.38	171.92	173.79	170.57
3	CC1P_3	0	3.34	23.07	45.68	68.15	94.08	146.91	169.78	183.41	181.14	184.02	201.10
3	CC1P_7	0	3.28	22.55	44.59	66.46	91.63	136.46	166.62	181.68	185.71	177.05	177.05
3	CC1P_11	0	3.23	22.15	43.73	65.11	89.69	133.44	164.28	179.07	181.74	177.32	180.92
3	CC1P_15	0	3.20	21.83	43.03	64.01	88.10	108.01	162.57	177.24	183.51	173.79	175.02
4	CC1P_4	0	3.41	23.55	46.64	69.59	96.05	142.77	171.35	185.88	193.32	190.08	205.94
4	CC1P_8	0	3.34	22.97	45.41	67.69	93.33	128.42	167.94	181.54	181.45	187.24	189.88
4	CC1P_12	0	3.29	22.49	44.41	66.13	91.10	113.21	165.09	178.65	179.96	182.90	184.63
4	CC1P_16	0	3.24	22.10	43.57	64.82	89.21	110.80	162.97	176.43	180.88	179.69	180.03
5	CC2P_1	0	3.61	23.75	45.63	66.59	111.24	114.19	114.32	113.10	126.79	124.40	----
5	CC2P_5	0	3.60	23.55	45.16	65.79	109.65	112.13	111.94	113.38	133.08	113.40	50.24

5	CC2P_9	0	3.59	23.42	44.82	65.20	108.26	113.76	113.37	110.97	126.21	110.64	95.19
5	CC2P_13	0	3.58	23.33	44.55	64.71	107.45	112.55	112.05	110.13	128.12	113.54	91.47
6	CC2P_2	0	3.63	23.58	45.07	65.54	88.36	121.59	124.32	123.04	143.45	129.65	103.29
6	CC2P_6	0	3.73	24.05	45.82	66.49	89.45	117.39	118.34	127.55	125.66	148.54	129.52
6	CC2P_10	0	3.67	23.55	44.73	64.77	86.96	116.96	117.32	128.29	119.51	136.07	118.98
6	CC2P_14	0	3.69	23.58	44.66	64.55	86.53	117.32	114.21	133.10	121.00	138.91	113.81
7	CC2P_3	0	3.94	25.30	48.21	70.06	94.43	115.49	130.20	131.34	150.83	143.06	142.03
7	CC2P_7	0	3.90	24.83	47.11	68.27	91.78	112.03	130.74	128.16	148.40	134.58	161.18
7	CC2P_11	0	3.87	24.49	46.28	66.88	89.71	109.33	131.70	124.88	143.57	148.07	150.17
7	CC2P_15	0	3.85	24.23	45.62	65.77	88.04	107.16	132.92	121.90	139.35	158.79	141.41
8	CC2P_4	0	3.94	25.17	47.93	69.68	93.98	115.01	139.09	133.25	155.10	142.26	136.31
8	CC2P_8	0	3.89	24.58	46.58	67.51	90.81	110.93	137.57	133.95	152.29	150.47	136.74
8	CC2P_12	0	3.85	24.13	45.51	65.78	88.28	107.67	138.05	131.08	150.96	140.53	146.36
8	CC2P_16	0	3.83	23.78	44.66	64.37	86.21	104.99	126.10	131.74	150.87	144.31	151.29
9	CC3P_1	0	3.24	21.34	41.04	59.88	98.15	99.35	94.70	107.73	118.99	106.97	99.76
9	CC3P_5	0	3.22	21.17	40.63	59.19	99.16	100.81	95.82	104.79	123.02	113.66	51.40
9	CC3P_9	0	3.21	21.05	40.33	58.66	98.19	102.14	98.58	100.35	116.21	112.39	89.36
9	CC3P_13	0	3.17	20.70	39.59	57.49	99.30	97.05	101.69	102.80	101.44	115.76	89.69
10	CC3P_2	0	3.36	21.77	41.44	60.02	80.53	108.10	104.09	105.55	123.09	110.89	102.95
10	CC3P_6	0	3.34	21.50	40.81	58.98	78.94	105.51	101.16	105.48	122.28	106.56	128.00
10	CC3P_10	0	3.32	21.31	40.35	58.18	77.73	108.45	104.97	100.49	114.92	101.26	115.07
10	CC3P_14	0	3.24	20.75	39.17	56.36	75.14	103.95	106.75	108.17	101.36	114.09	97.05
11	CC3P_3	0	3.31	21.08	39.81	57.39	76.71	114.39	114.24	118.30	115.38	112.83	104.24
11	CC3P_7	0	3.28	20.72	38.97	56.02	74.65	90.50	112.14	115.61	114.83	114.39	120.97
11	CC3P_11	0	3.25	20.47	38.35	54.96	73.06	88.41	110.84	114.30	115.59	110.78	111.80
11	CC3P_15	0	3.31	20.76	38.77	55.44	73.54	88.87	112.64	112.38	107.91	120.01	112.25
12	CC3P_4	0	3.38	21.22	39.91	57.46	76.76	93.27	122.56	125.09	124.53	132.14	128.41
12	CC3P_8	0	3.34	20.76	38.83	55.70	74.16	89.90	122.45	121.58	120.30	136.01	131.52
12	CC3P_12	0	3.31	20.42	38.01	54.34	72.13	87.25	123.49	121.59	117.43	125.69	135.30
12	CC3P_16	0	3.37	20.72	38.38	54.70	72.42	87.46	102.20	120.94	119.95	123.84	135.37

Table T3. S/N ratio for Slope characteristics

Level	Expt no	Slope (β)	β^2	S/N ratio (η)	Level	Expt no	Slope (β)	β^2	S/N ratio (η)
1	CC1P_1	0.717	0.514	-2.89	7	CC2P_3	0.767	0.588	-2.30
1	CC1P_5	0.705	0.497	-3.04	7	CC2P_7	0.747	0.558	-2.53
1	CC1P_9	0.695	0.483	-3.16	7	CC2P_11	0.731	0.534	-2.72
1	CC1P_13	0.690	0.476	-3.22	7	CC2P_15	0.718	0.516	-2.88
2	CC1P_2	0.736	0.542	-2.66	8	CC2P_4	0.763	0.582	-2.35
2	CC1P_6	0.720	0.518	-2.85	8	CC2P_8	0.738	0.545	-2.64
2	CC1P_10	0.708	0.501	-3.00	8	CC2P_12	0.718	0.516	-2.88
2	CC1P_14	0.698	0.487	-3.12	8	CC2P_16	0.702	0.493	-3.07
3	CC1P_3	0.753	0.567	-2.46	9	CC3P_1	0.657	0.432	-3.65
3	CC1P_7	0.734	0.539	-2.69	9	CC3P_5	0.650	0.423	-3.74
3	CC1P_11	0.719	0.517	-2.87	9	CC3P_9	0.644	0.415	-3.82
3	CC1P_15	0.706	0.498	-3.02	9	CC3P_13	0.630	0.397	-4.01
4	CC1P_4	0.769	0.591	-2.28	10	CC3P_2	0.657	0.432	-3.65
4	CC1P_8	0.748	0.560	-2.52	10	CC3P_6	0.646	0.417	-3.80
4	CC1P_12	0.730	0.533	-2.73	10	CC3P_10	0.636	0.404	-3.93
4	CC1P_16	0.715	0.511	-2.91	10	CC3P_14	0.614	0.377	-4.24
5	CC2P_1	0.731	0.534	-2.72	11	CC3P_3	0.627	0.393	-4.05
5	CC2P_5	0.722	0.521	-2.83	11	CC3P_7	0.612	0.375	-4.26
5	CC2P_9	0.715	0.511	-2.91	11	CC3P_11	0.600	0.360	-4.44
5	CC2P_13	0.709	0.503	-2.99	11	CC3P_15	0.599	0.359	-4.45
6	CC2P_2	0.719	0.517	-2.87	12	CC3P_4	0.627	0.393	-4.05
6	CC2P_6	0.728	0.530	-2.76	12	CC3P_8	0.607	0.368	-4.34
6	CC2P_10	0.709	0.503	-2.99	12	CC3P_12	0.591	0.349	-4.57
6	CC2P_14	0.706	0.498	-3.02	12	CC3P_16	0.588	0.346	-4.61

Table T4. S/N ratio for volume

Level	Expt no	Volume (V)	V^2	S/N ratio (η)	Level	Expt no	Volume (V)	V^2	S/N ratio (η)

1	CC1P_1	378.0	142884	-51.550	7	CC2P_3	846.0	715716	-58.547
1	CC1P_5	453.6	205753	-53.133	7	CC2P_7	1015.2	1030631	-60.131
1	CC1P_9	529.2	280052.6	-54.472	7	CC2P_11	1184.4	1402803	-61.470
1	CC1P_13	604.8	365783	-55.632	7	CC2P_15	1353.6	1832233	-62.630
2	CC1P_2	480.0	230400	-53.625	8	CC2P_4	1014.0	1028196	-60.121
2	CC1P_6	576.0	331776	-55.208	8	CC2P_8	1216.8	1480602	-61.704
2	CC1P_10	672.0	451584	-56.547	8	CC2P_12	1419.6	2015264	-63.043
2	CC1P_14	768.0	589824	-57.707	8	CC2P_16	1622.4	2632182	-64.203
3	CC1P_3	582.0	338724	-55.298	9	CC3P_1	576.0	331776	-55.208
3	CC1P_7	698.4	487762.6	-56.882	9	CC3P_5	691.2	477757.4	-56.792
3	CC1P_11	814.8	663899	-58.221	9	CC3P_9	806.4	650281	-58.131
3	CC1P_15	931.2	867133.4	-59.381	9	CC3P_13	921.6	849346.6	-59.291
4	CC1P_4	684.0	467856	-56.701	10	CC3P_2	810.0	656100	-58.170
4	CC1P_8	820.8	673712.6	-58.285	10	CC3P_6	972.0	944784	-59.753
4	CC1P_12	957.6	916997.8	-59.624	10	CC3P_10	1134.0	1285956	-61.092
4	CC1P_16	1094.4	1197711	-60.784	10	CC3P_14	1296.0	1679616	-62.252
5	CC2P_1	510.0	260100	-54.151	11	CC3P_3	1044.0	1089936	-60.374
5	CC2P_5	612.0	374544	-55.735	11	CC3P_7	1252.8	1569508	-61.958
5	CC2P_9	714.0	509796	-57.074	11	CC3P_11	1461.6	2136275	-63.297
5	CC2P_13	816.0	665856	-58.234	11	CC3P_15	1670.4	2790236	-64.456
6	CC2P_2	678.0	459684	-56.625	12	CC3P_4	1278.0	1633284	-62.131
6	CC2P_6	813.6	661945	-58.208	12	CC3P_8	1533.6	2351929	-63.714
6	CC2P_10	949.2	900980.6	-59.547	12	CC3P_12	1789.2	3201237	-65.053
6	CC2P_14	1084.8	1176791	-60.707	12	CC3P_16	2044.8	4181207	-66.213

Table T5. S/N ratio for the critical load

Level	Expt no	P_c (MPa)	$1 / P_c^2$	S/N ratio (η)	Level	Expt no	P_c (MPa)	$1 / P_c^2$	S/N ratio (η)
1	CC1P_1	268.88	72296.454	1.3832E-05	7	CC2P_3	326.56	106641.43	9.3772E-06
1	CC1P_5	279.6	78176.16	1.2792E-05	7	CC2P_7	337.34	113798.28	8.7875E-06
1	CC1P_9	286.84	82277.186	1.2154E-05	7	CC2P_11	337.81	114115.6	8.763E-06
1	CC1P_13	292.08	85310.726	1.1722E-05	7	CC2P_15	337.99	114237.24	8.7537E-06
2	CC1P_2	285.2	81339.04	1.2294E-05	8	CC2P_4	336.63	113319.76	8.8246E-06
2	CC1P_6	304.91	92970.108	1.0756E-05	8	CC2P_8	337.5	113906.25	8.7791E-06
2	CC1P_10	320.54	102745.89	9.7327E-06	8	CC2P_12	337.77	114088.57	8.7651E-06
2	CC1P_14	332.8	110755.84	9.0289E-06	8	CC2P_16	338.05	114277.8	8.7506E-06
3	CC1P_3	294.28	86600.718	1.1547E-05	9	CC3P_1	271	73441	1.3616E-05
3	CC1P_7	327.66	107361.08	9.3144E-06	9	CC3P_5	298.95	89371.103	1.1189E-05
3	CC1P_11	338.61	114656.73	8.7217E-06	9	CC3P_9	308.85	95388.323	1.0483E-05
3	CC1P_15	338.7	114717.69	8.7171E-06	9	CC3P_13	315.98	99843.36	1.0016E-05
4	CC1P_4	301.38	90829.904	1.101E-05	10	CC3P_2	308.25	95018.063	1.0524E-05
4	CC1P_8	338.46	114555.17	8.7294E-06	10	CC3P_6	336	112896	8.8577E-06
4	CC1P_12	338.64	114677.05	8.7201E-06	10	CC3P_10	337.77	114088.57	8.7651E-06
4	CC1P_16	338.92	114866.77	8.7057E-06	10	CC3P_14	337.36	113811.77	8.7864E-06
5	CC2P_1	276.8	76618.24	1.3052E-05	11	CC3P_3	325.23	105774.55	9.4541E-06
5	CC2P_5	292.8	85731.84	1.1664E-05	11	CC3P_7	337.35	113805.02	8.787E-06
5	CC2P_9	304.91	92970.108	1.0756E-05	11	CC3P_11	337.77	114088.57	8.7651E-06
5	CC2P_13	310.83	96615.289	1.035E-05	11	CC3P_15	337.8	114108.84	8.7636E-06
6	CC2P_2	297.68	88613.382	1.1285E-05	12	CC3P_4	336.45	113198.6	8.834E-06
6	CC2P_6	320.4	102656.16	9.7413E-06	12	CC3P_8	337.35	113805.02	8.787E-06
6	CC2P_10	337.53	113926.5	8.7776E-06	12	CC3P_12	337.81	114115.6	8.763E-06
6	CC2P_14	337.89	114169.65	8.7589E-06	12	CC3P_16	337.97	114223.72	8.7547E-06